

Driving skyrmions with low threshold current density in amorphous CoFeB thin film

Brindaban Ojha,^{1,*} Sougata Mallick,^{2,*} Minaxi Sharma,¹ André Thiaville,² Stanislas Rohart,^{2,†} and Subhankar Bedanta^{1,‡}

¹*Laboratory for Nanomagnetism and Magnetic Materials (LNMM), School of Physical Sciences, National Institute of Science Education and Research (NISER), HBNI, Jatni-752050, Odisha, India*

²*Laboratoire de Physique des Solides, Université Paris-Saclay, CNRS UMR 8502, F-91405 Orsay Cedex, France*

(Dated: June 7, 2021)

Magnetic skyrmions are topologically stable spin swirling particle like entities which are appealing for next generation spintronic devices. The expected low critical current density for the motion of skyrmions makes them potential candidates for future energy efficient electronic devices. Several heavy metal/ferromagnetic (HM/FM) systems have been explored in the past decade to achieve faster skyrmion velocity at low current densities. In this context, we have studied Pt/CoFeB/MgO heterostructures in which skyrmions have been stabilized at room temperature (RT). It has been observed that the shape of the skyrmions are perturbed even by the small stray field arising from low moment magnetic tips while performing the magnetic force microscopy (MFM), indicating presence of low pinning landscape in the samples. This hypothesis is indeed confirmed by the low threshold current density to drive the skyrmions in our sample, at velocities of few 10 m/s.

Keywords: Perpendicular magnetic anisotropy, Dzyaloshinskii-Moriya interaction (DMI), skyrmions, thinfilm

INTRODUCTION

Since the proposition of employing skyrmions (chiral textures obtained in material with broken inversion symmetry) in spintronic devices [1], a collective research effort has addressed the key aspects of this subject. Nanoscale dimension, fascinating topological property, and potentially low threshold current density (in comparison to the domain walls, DWs) to drive the skyrmions, make them promising candidates for logic and storage technology [1–8]. In the experimental perspective, there are three major challenges: (i) stabilization of skyrmions at room temperature, (ii) deterministic nucleation of skyrmions, and (iii) efficient motion of skyrmions under spin Hall effect (SHE). Over the last decade, many experimental works [9–15] have been focused in the aforementioned directions to achieve the ambitious goal of skyrmion based device applications. However, controlled nucleation and motion of individual skyrmions in nanotracks with low power consumption still remains a challenge.

Due to Heisenberg exchange interaction, ferromagnetic materials principally exhibit collinear ordering between neighbouring spins. However, the presence of large spin-orbit coupling and Dzyaloshinskii-Moriya interaction (DMI) due to broken symmetry can lead to stabilization of non-collinear spin textures viz. skyrmions [11–14, 16]. This combination also enables the spin-orbit torque (SOT) to efficiently manipulate the magnetization. Further, DMI lowers the total DW energy. The most widely used combination for such system is a heterostructure of heavy metal (HM)/ferromagnet (FM)/oxide (O) [12–14]. Recent works have revealed that the skyrmions can be stabilized, nucleated, and driven using external magnetic field [13, 14], electrical

field [17, 18], spin polarized current pulses [9, 13, 14, 19], local field gradient [20, 21], anisotropy gradient [22], etc. Nevertheless, a crucial criterion for device applications is a low power to drive the skyrmions. This makes materials with low pinning energy landscape indispensable. However, in spite of several works in this field, the required threshold current density to drive the skyrmions is yet to reach the desired limit for real-life applications.

In this context, we chose the combination of Pt/Co₄₀Fe₄₀B₂₀/MgO to investigate the current driven dynamics of the skyrmions under the influence of SOT. Amorphous CoFeB has been selected as the FM layer since the absence of grain boundaries results in lower pinning in comparison to polycrystalline FM layers (viz., Co, Fe, etc.) [14]. Brillouin light scattering (BLS) measurements [23–26] have been performed to quantify the DMI in the samples. We show with static magnetic force microscopy imaging that skyrmions can be stabilized at room temperature under external magnetic field. The shape of the skyrmions is significantly perturbed even by the stray field of ultralow moment magnetic tips indicating a low pinning soft magnetic material. It is also shown that the required threshold current density to drive the skyrmions at velocities compatible with applications (>10 m/s) is significantly low in comparison to the state of art.

EXPERIMENTAL DETAILS

We have prepared Ta (5 nm)/Pt (6 nm)/Co₄₀Fe₄₀B₂₀ (t_{CoFeB})/MgO (2 nm)/Ta (3 nm) heterostructure on thermally oxidized Si/SiO₂(100 nm) substrates. The schematic of the sample structure is shown in Fig. 1(a). We choose SiO₂ 100 nm since it leads to better signal

in the optical measurements [27]. A Ta seed layer has been chosen to promote the (111) growth of Pt as well as to reduce the strain between Pt and the substrate. We also use a 3nm Ta on the top as a capping layer. The thickness of CoFeB has been varied between 1.1 to 1.9 nm. The samples are named as S1, S2, S3, S4, S5, S6 and S7 for $t_{CoFeB} = 1.1, 1.2, 1.5, 1.6, 1.7, 1.75$ and 1.9 nm, respectively. The sample preparation was performed in a high-vacuum chamber consisting of sputtering and e-beam evaporators. The base pressure of the chamber was better than 8×10^{-8} mbar. Ta, Pt, and CoFeB layers were deposited using DC magnetron sputtering while e-beam evaporation technique was employed to prepare MgO. The substrate has been rotated with 10 rpm during deposition to improve uniformity of the layers. In order to promote the interfacial perpendicular magnetic anisotropy (PMA), all the samples were annealed *in situ* at 600°C for 1 hour in vacuum ($\sim 1 \times 10^{-7}$), after deposition. Fig. 1(a) shows the schematic of the thin film heterostructure. To quantify the spontaneous magnetization (M_s) of the samples we have performed hysteresis measurements via a superconducting quantum interference device (SQUID) magnetometer. Microfabrication of the tracks and the contacts in the samples has been performed using a two-step electron beam lithography (EBL) and Ar ion etching. We deposited Ti (5 nm) and Au (50 nm) contact pads for transport measurements using e-beam evaporation. The imaging of skyrmions and their dynamics under the application of current has been performed by magnetic force microscopy (MFM) using homemade CoCr/Cr tip coating, to minimize tip induced perturbations. BLS measurements have been performed in Damon-Eshbach geometry [23–26] to quantify the interfacial DMI (iDMI) in the samples.

RESULTS AND DISCUSSION

The MOKE measurements (shown in Fig. S1 in the supplementary information) confirm that the samples S1, S2, S3 and S4 are out-of-plane (OOP) magnetized while samples S5, S6 and S7 are in-plane (IP) magnetized. To get further insight about anisotropy we have deduced the effective anisotropy (K_{eff}) constant using the relation $K_{eff} = -\frac{1}{2}H_s M_s$ (negative sign indicates the IP anisotropy), where H_s and M_s are saturation field, and spontaneous magnetization, respectively. The calculation of H_s is shown in supplementary information. The M_s value of Pt/CoFeB/MgO film is 1.58×10^6 A/m. A dead layer of thickness (t_d) ~ 0.4 nm is observed in the samples (calculated from $M_s \times t_{CoFeB}$ vs t_{CoFeB} plot, shown in Fig. S3 of the supplementary information). Here, the dead layer appears possibly due to the intermixing at Pt/CoFeB interface and oxidation at CoFeB/MgO interface.

Fig. 1 (b) shows the plot of $K_{eff} t_{CoFeB}$ vs t_{CoFeB} .

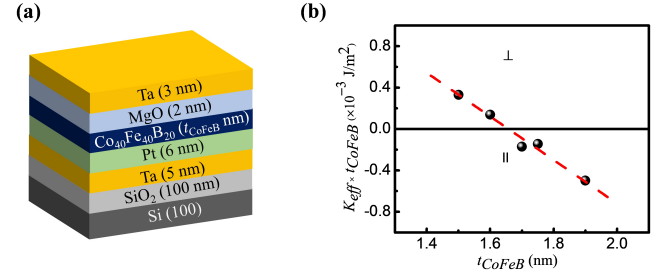


FIG. 1. (a) Schematic of sample structure. (b) Plot of $K_{eff} t_{CoFeB}$ vs t_{CoFeB} and fit (red dashed line) using equation 1.

The experimental data (black dots) of this plot is fitted (red dashed line) using straight line fitting [26]:

$$K_{eff} t_{CoFeB} = K_V t_{CoFeB} + K_S \quad (1)$$

where K_V and K_S are volume and surface contributions of anisotropy, respectively. In fig. 1(b) the slope and intercept correspond to K_V and K_S which are -2.10 MJ/m³ and 3.48 mJ/m², respectively. Here, K_V includes the shape anisotropy and K_S is the sum of two surface anisotropies arising from Pt/CoFeB and CoFeB/MgO interfaces. The best fit of Fig. 1(b) intersects the x-axis at $t_{CoFeB} = 1.65$ nm depicting the occurrence of spin reorientation transition (SRT). We have performed the BLS measurements to quantify the iDMI of the samples. The detailed analysis of calculating the iDMI values from the BLS measurements is shown in the supplementary information. The iDMI constants are 0.4 ± 0.02 mJ/m² for S3 and S4.

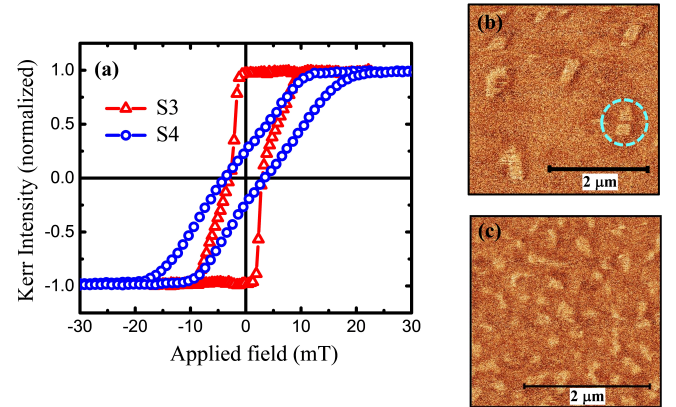


FIG. 2. (a) Hysteresis loop of sample S3 (red) and S4 (blue) in polar MOKE. (b) [resp. (c)] MFM images of samples S3 [resp. S4] at applied fields of 1 mT [resp. 3 mT]. The cyan circled area in (b) shows the distorted shape of the skyrmion induced by the tip perturbation.

In order to stabilize isolated skyrmions, we need to fine tune the DW energy [16] between two limiting cases: (a) a large positive energy which causes the collapse

of the skyrmions, and (b) a large negative wall energy which destabilizes the collinear order, leading to isolated skyrmions only at large external magnetic field [19]. One way of achieving this is to keep the FM layer thickness near the SRT to reduce the effective anisotropy energy of the system to near zero. This is confirmed by the presence of skyrmionic states in samples S3 and S4 as observed using MFM. Fig. 2(a) shows the corresponding hysteresis loops of samples S3 (red curve) and S4 (blue curve). Wormlike stripe domains are observed in the demagnetized state indicating that the ground state is 1D textures. By applying OOP fields of 1 and 3 mT (Fig. 2(b) and (c)), isolated skyrmions have been observed in the sample S3, and S4, respectively. The average size of the skyrmions (measured within the accuracy of the MFM) varies in the range of 200-500 nm and 150-300 nm for samples S3 and S4, respectively. We should note from fig. 2 (b), and (c) that the shape of the skyrmions is significantly perturbed (for reference see cyan circled section of fig. 2(b)) even by the stray field of the lowest moment magnetic tips. This indicates the presence of low pinning landscape in the amorphous CoFeB.

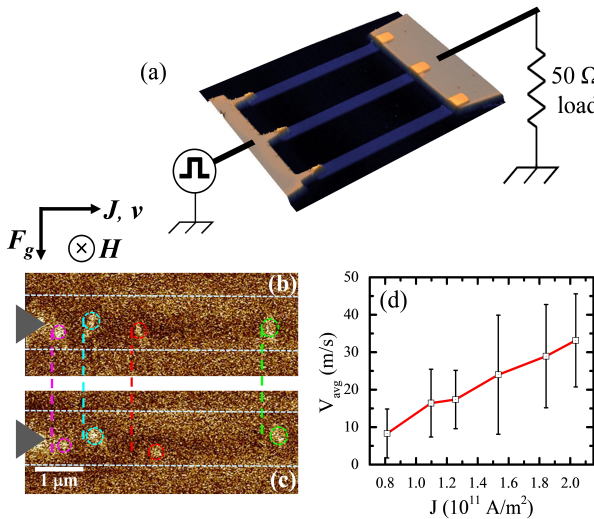


FIG. 3. (a) Schematic of the set-up for current induced motion experiment with the AFM image of three $1\mu\text{m}$ wide nanotracks (blue) with Ti/Au contacts (light brown) microfabricated on sample S3 (CoFeB: 1.5 nm). (b) and (c) show the position (by coloured circles) and displacement (by coloured lines) of the skyrmions before and after application of one current pulse. The white dashed lines are indicating the boundary of a single nanotrack in the MFM image. Aboves these images, the arrows indicates the current J , velocity v , applied field H and gyrotropic deflection force $F_g = G \times v$ (where G is the skyrmion gyrovector). (d) shows the average skyrmion velocity as a function of different applied current density.

Sample S3 is selected for the study of current-induced dynamics due to its potentially low pinning energy landscape and better control under applied magnetic field. We start from the demagnetized state and apply perpen-

dicular magnetic field of 1.0 mT (along $-\hat{z}$) to stabilize the skyrmions in the tracks. Subsequently, we apply 20 ns current pulses with increasing amplitude. Fig. 3(a) shows the schematic of the sample structure with the AFM images of the nanotracks (3 parallel tracks with width $\sim 1.2\text{ }\mu\text{m}$ separated by $\sim 2.8\text{ }\mu\text{m}$ from each other) along with Ti/Au contact pads. The current is injected in the tracks using the point-like contacts on the left and collected at the common ground. Beyond a threshold current density of $\sim 0.8 \times 10^{11}\text{ A/m}^2$, the skyrmions start moving in the track. The motion of the skyrmions, opposite to the electron motion direction, confirms the dynamics due to SOT [9]. The skyrmion velocity as a function of applied current density is measured by calculating the average displacement of all the skyrmions present in the track. Fig. 3(b) and (c) show the skyrmion displacements marked by different colours before and after the application of one current pulse. It should be noted that both at lower as well as at higher current densities, the displacements of all the skyrmions are not equal. This is the consequence of the skyrmion hopping due to the presence of defects within the potential landscape [36]. The skyrmions advance in the track until they are either pinned or face strong skyrmion-skyrmion repulsion from another pinned skyrmion. We also note a tendency for the skyrmions to derive toward their right, which is an indication of their topological nature, through a gyrotropic deflection [19, 29]. Hence, we plot the average velocity of all the skyrmions present in the track for a particular current density (Fig. 3(d)). The error bar in Fig. 3(d) corresponds to the difference between highest and lowest skyrmion displacement. We obtain the highest skyrmion velocity of 46 m/s for a current density of $\sim 2 \times 10^{11}\text{ A/m}^2$. Application of higher current densities led to burning of the contacts due to application of large ($\sim 20\text{ ns}$) current pulses through the tracks (see Fig. S6 in supplementary information for details). The threshold current density reported in this work is lower than the ones reported in the literature (see Table 1), while giving access to velocities of few 10 m/s slightly above, among the best reports.

CONCLUSION

In conclusion, we have shown that skyrmions are stabilized at very low field in Pt/CoFeB/MgO heterostructures at room temperature. We have quantified the iDMI value for our thin films which is similar to earlier reports. We observe significantly lower threshold current densities to drive the skyrmions. Larger skyrmion velocity under shorter current pulses can be expected in similar samples. We believe that the work presented here may be helpful to utilize such low pinning amorphous materials for skyrmionic applications at low power consumption.

TABLE I. Comparison of threshold current density with existing literature at room temperature. Two groups of results can be distinguished. In the first one, the measured velocities are well below 1 m/s, while in the second one, the velocities are larger than 10 m/s. In the second group, that concerns the fastest skyrmion, our work displays the smallest threshold current density.

Group	Authors	Sample structure	Threshold current density (A/m^2)	Velocity range (m/s)
1	Jiang <i>et al.</i> [13]	Ta/CoFeB/TaO _x	1.5×10^8	$(2.5 - 25) \times 10^{-6}$
	Yu <i>et al.</i> [28]	Ta/CoFeB/TaO _x	3.5×10^9	0.2 – 0.4
	Jiang <i>et al.</i> [29]	Ta/CoFeB/TaO _x	6×10^9	0.01 – 0.75
	Tolley <i>et al.</i> [30]	Ta/Pt/Co/Os/Pt/Ta	2.0×10^8	$(2.5 - 13) \times 10^{-6}$
2	Woo <i>et al.</i> [14]	[Pt/Co/Ta] ₁₅ ; [Pt/CoFeB/MgO] ₁₅	2.0×10^{11}	1–45; 1–100
	Legrand <i>et al.</i> [31]	Ta/Co/[Pt/Ir/Co] ₁₀ /Pt	2.38×10^{11}	15 – 47
	Hrabec <i>et al.</i> [19]	Pt/FM/Au/FM/Pt, FM = Ni/Co/Ni	2.6×10^{11}	10 – 60
	Woo <i>et al.</i> [32]	Ta/[Pt/CoFeB/MgO] ₂₀ /Ta	1.5×10^{11}	5 – 40
	Akhtar <i>et al.</i> [33]	Ta/Pt/CFA/MgO/Ta	1.6×10^{11}	10
	Juge <i>et al.</i> [34]	Ta/Pt/Co/MgO/Ta	3.5×10^{11}	15 – 100
	Litzius <i>et al.</i> [35]	[Pt/CoFeB/MgO] ₁₅	3.2×10^{11}	1 – 35
	This work	Ta/Pt/CoFeB/MgO/Ta	0.8×10^{11}	9 – 46

ACKNOWLEDGMENTS

The authors thank DAE, Govt. of India and the Indo-French collaborative project supported by CEFIPRA (IFC/5808-1/2017), and the French National Research Agency (ANR) (Topsky, ANR-17-CE24-0025) for providing the research funding. The BLS setup was funded by the PHOM and EOE Research Departments of Université Paris-Saclay, CNRS-Institut de Physique, French National Research Agency (ANR) as part of the “Investissements d’Avenir” program (Labex NanoSaclay, ANR-10-LABX-0035) through the BLS@Psay and SPICY projects, and Ile-de-France region through the SESAME IMAGeSPIN (EX039175) project. We would like to thank Dr. Braj Bhushan Singh for the help in SQUID measurements and valuable discussion. We would also like to thank Raphael Weil for his help in microfabrication.

- [4] G. Yu, P. Upadhyaya, X. Li, W. Li, S. K. Kim, Y. Fan, K. L. Wong, Y. Tserkovnyak, P. K. Amiri, and K. L. Wang, Room-temperature creation and spin-orbit torque manipulation of skyrmions in thin films with engineered asymmetry, *Nano letters* **16**, 1981 (2016).
- [5] X. Zhang, G. Zhao, H. Fangohr, J. P. Liu, W. Xia, J. Xia, and F. Morvan, Skyrmion-skyrmion and skyrmion-edge repulsions in skyrmion-based racetrack memory, *Scientific reports* **5**, 7643 (2015).
- [6] A. Fert, N. Reyren, and V. Cros, Magnetic skyrmions: advances in physics and potential applications, *Nature Reviews Materials* **2**, 17031 (2017).
- [7] W. Kang, Y. Huang, C. Zheng, W. Lv, N. Lei, Y. Zhang, X. Zhang, Y. Zhou, and W. Zhao, Voltage controlled magnetic skyrmion motion for racetrack memory, *Scientific reports* **6**, 23164 (2016).
- [8] S. Zhang, J. Wang, Q. Zheng, Q. Zhu, X. Liu, S. Chen, C. Jin, Q. Liu, C. Jia, and D. Xue, Current-induced magnetic skyrmions oscillator, *New Journal of Physics* **17**, 023061 (2015).
- [9] J. Sampaio, V. Cros, S. Rohart, A. Thiaville, and A. Fert, Nucleation, stability and current-induced motion of isolated magnetic skyrmions in nanostructures, *Nature nanotechnology* **8**, 839 (2013).
- [10] D. Maccariello, W. Legrand, N. Reyren, K. Garcia, K. Bouzehouane, S. Collin, V. Cros, and A. Fert, Electrical detection of single magnetic skyrmions in metallic multilayers at room temperature, *Nature nanotechnology* **13**, 233 (2018).
- [11] A. Soumyanarayanan, M. Raju, A. G. Oyarce, A. K. Tan, M.-Y. Im, A. Petrović, P. Ho, K. Khoo, M. Tran, C. Gan, et al., Tunable room-temperature magnetic skyrmions in ir/fe/co/pt multilayers, *Nature materials* **16**, 898 (2017).
- [12] O. Boulle, J. Vogel, H. Yang, S. Pizzini, D. de Souza Chaves, A. Locatelli, T. O. Mentes, A. Sala, L. D. Buda-Prejbeanu, O. Klein, et al., Room-temperature chiral magnetic skyrmions in ultrathin

* These authors contributed equally to this work

† stanislas.rohart@universite-paris-saclay.fr

‡ sbedanta@niser.ac.in

- [1] A. Fert, V. Cros, and J. Sampaio, Skyrmions on the track, *Nature nanotechnology* **8**, 152 (2013).
- [2] W. Koshiba, Y. Kaneko, J. Iwasaki, M. Kawasaki, Y. Tokura, and N. Nagaosa, Memory functions of magnetic skyrmions, *Japanese Journal of Applied Physics* **54**, 053001 (2015).
- [3] R. Tomasello, E. Martinez, R. Zivieri, L. Torres, M. Carpentieri, and G. Finocchio, A strategy for the design of skyrmion racetrack memories, *Scientific reports* **4**, 6784 (2014).

- magnetic nanostructures, *Nature nanotechnology* **11**, 449 (2016).
- [13] W. Jiang, P. Upadhyaya, W. Zhang, G. Yu, M. B. Jungfleisch, F. Y. Fradin, J. E. Pearson, Y. Tserkovnyak, K. L. Wang, O. Heinonen, et al., Blowing magnetic skyrmion bubbles, *Science* **349**, 283 (2015).
- [14] S. Woo, K. Litzius, B. Krüger, M.-Y. Im, L. Caretta, K. Richter, M. Mann, A. Krone, R. M. Reeve, M. Weigand, et al., Observation of room-temperature magnetic skyrmions and their current-driven dynamics in ultrathin metallic ferromagnets, *Nature materials* **15**, 501 (2016).
- [15] Y. Zhou and M. Ezawa, A reversible conversion between a skyrmion and a domain-wall pair in a junction geometry, *Nature communications* **5**, 4652 (2014).
- [16] S. Rohart and A. Thiaville, Skyrmion confinement in ultrathin film nanostructures in the presence of dzyaloshinskii-moriya interaction, *Physical Review B* **88**, 184422 (2013).
- [17] C. Ma, X. Zhang, J. Xia, M. Ezawa, W. Jiang, T. Ono, S. Piramanayagam, A. Morisako, Y. Zhou, and X. Liu, Electric field-induced creation and directional motion of domain walls and skyrmion bubbles, *Nano letters* **19**, 353 (2018).
- [18] M. Schott, A. Bernand-Mantel, L. Ranno, S. Pizzini, J. Vogel, H. Béa, C. Baraduc, S. Auffret, G. Gaudin, and D. Givord, The skyrmion switch: turning magnetic skyrmion bubbles on and off with an electric field, *Nano letters* **17**, 3006 (2017).
- [19] A. Hrabec, J. Sampaio, M. Belmeguenai, I. Gross, R. Weil, S. M. Chérif, A. Stashkevich, V. Jacques, A. Thiaville, and S. Rohart, Current-induced skyrmion generation and dynamics in symmetric bilayers, *Nature communications* **8**, 15765 (2017).
- [20] R. Tomasello, S. Komineas, G. Siracusano, M. Carpenteri, and G. Finocchio, Chiral skyrmions in an anisotropy gradient, *Physical Review B* **98**, 024421 (2018).
- [21] F. Büttner, C. Moutafis, M. Schneider, B. Krüger, C. Günther, J. Geilhufe, C. v. K. Schmising, J. Mohanty, B. Pfau, S. Schaffert, et al., Dynamics and inertia of skyrmionic spin structures, *Nature Physics* **11**, 225 (2015).
- [22] A. Casiraghi, H. Corte-León, M. Vafaei, F. Garcia-Sánchez, G. Durin, M. Pasquale, G. Jakob, M. Kläui, and O. Kazakova, Individual skyrmion manipulation by local magnetic field gradients, *Communications Physics* **2**, 145 (2019).
- [23] M. Belmeguenai, J.-P. Adam, Y. Roussigné, S. Eimer, T. Devolder, J.-V. Kim, S. M. Cherif, A. Stashkevich, and A. Thiaville, Interfacial dzyaloshinskii-moriya interaction in perpendicularly magnetized pt/co/alo x ultrathin films measured by brillouin light spectroscopy, *Physical Review B* **91**, 180405 (2015).
- [24] S. Tacchi, R. Troncoso, M. Ahlberg, G. Gubbiotti, M. Madami, J. Åkerman, and P. Landeros, Interfacial dzyaloshinskii-moriya interaction in pt/cofeb films: Effect of the heavy-metal thickness, *Physical review letters* **118**, 147201 (2017).
- [25] K. Di, V. L. Zhang, H. S. Lim, S. C. Ng, M. H. Kuok, X. Qiu, and H. Yang, Asymmetric spin-wave dispersion due to dzyaloshinskii-moriya interaction in an ultrathin pt/cofeb film, *Applied Physics Letters* **106**, 052403 (2015).
- [26] M. Belmeguenai, Y. Roussigné, H. Bouloussa, S. Chérif, A. Stashkevich, M. Nasui, M. Gabor, A. Mora-Hernández, B. Nicholson, O.-O. Inyang, et al., Thickness dependence of the dzyaloshinskii-moriya interaction in co 2 feal ultrathin films: Effects of annealing temperature and heavy-metal material, *Physical Review Applied* **9**, 044044 (2018).
- [27] A. Hrabec, M. Belmeguenai, A. Stashkevich, S. Chérif, S. Rohart, Y. Roussigné, and A. Thiaville, Making the dzyaloshinskii-moriya interaction visible, *Applied Physics Letters* **110**, 242402 (2017).
- [28] G. Yu, P. Upadhyaya, Q. Shao, H. Wu, G. Yin, X. Li, C. He, W. Jiang, X. Han, P. K. Amiri, et al., Room-temperature skyrmion shift device for memory application, *Nano letters* **17**, 261 (2017).
- [29] W. Jiang, X. Zhang, G. Yu, W. Zhang, X. Wang, M. B. Jungfleisch, J. E. Pearson, X. Cheng, O. Heinonen, K. L. Wang, et al., Direct observation of the skyrmion hall effect, *Nature Physics* **13**, 162 (2017).
- [30] R. Tolley, S. Montoya, and E. Fullerton, Room-temperature observation and current control of skyrmions in pt/co/os/pt thin films, *Physical Review Materials* **2**, 044404 (2018).
- [31] W. Legrand, D. Maccariello, N. Reyren, K. Garcia, C. Moutafis, C. Moreau-Luchaire, S. Collin, K. Bouzehouane, V. Cros, and A. Fert, Room-temperature current-induced generation and motion of sub-100 nm skyrmions, *Nano letters* **17**, 2703 (2017).
- [32] S. Woo, K. M. Song, H.-S. Han, M.-S. Jung, M.-Y. Im, K.-S. Lee, K. S. Song, P. Fischer, J.-I. Hong, J. W. Choi, et al., Spin-orbit torque-driven skyrmion dynamics revealed by time-resolved x-ray microscopy, *Nature communications* **8**, 15573 (2017).
- [33] W. Akhtar, A. Hrabec, S. Chouaib, A. Haykal, I. Gross, M. Belmeguenai, M. Gabor, B. Shields, P. Maletinsky, A. Thiaville, et al., Current-induced nucleation and dynamics of skyrmions in a co-based heusler alloy, *Physical Review Applied* **11**, 034066 (2019).
- [34] R. Juge, S.-G. Je, D. de Souza Chaves, L. D. Budapesteanu, J. Peña-Garcia, J. Nath, I. M. Miron, K. G. Rana, L. Aballe, M. Foerster, et al., Current-driven skyrmion dynamics and drive-dependent skyrmion hall effect in an ultrathin film, *Physical Review Applied* **12**, 044007 (2019).
- [35] K. Litzius, J. Leliaert, P. Bassirian, D. Rodrigues, S. Kromin, I. Lemesh, J. Zazvorka, K.-J. Lee, J. Mulders, N. Kerber, et al., The role of temperature and drive current in skyrmion dynamics, *Nature Electronics* **3**, 30 (2020).
- [36] K.-J. Kim, J.-C. Lee, S.-M. Ahn, K.-S. Lee, C.-W. Lee, Y. J. Cho, S. Seo, K.-H. Shin, S.-B. Choe, and H.-W. Lee, Interdimensional universality of dynamic interfaces, *Nature* **458**, 740 (2009).

Supplementary information

Driving skyrmions with low threshold current density in amorphous CoFeB thin film

Brindaban Ojha,^{1,*} Sougata Mallick,^{2,*} Minaxi Sharma,¹ André Thiaville,² Stanislas Rohart,^{2,†} and Subhankar Bedanta^{1,‡}

¹*Laboratory for Nanomagnetism and Magnetic Materials (LNMM), School of Physical Sciences, National Institute of Science Education and Research (NISER), HBNI, Jatni-752050, Odisha, India*

²*Laboratoire de Physique des Solides, Université Paris-Saclay,*

CNRS UMR 8502, F-91405 Orsay Cedex, France

(Dated: June 7, 2021)

Fig. S1 shows the hysteresis loops of the samples measured by MOKE microscope. The easy axis of the magnetization of samples S1, S2, S3 and S4 (Fig. S1(a)) is oriented along out-of-plane (OOP) direction. The samples S5, S6 and S7 show an easy axis along in-plane (IP) direction (Fig. S1(b)).

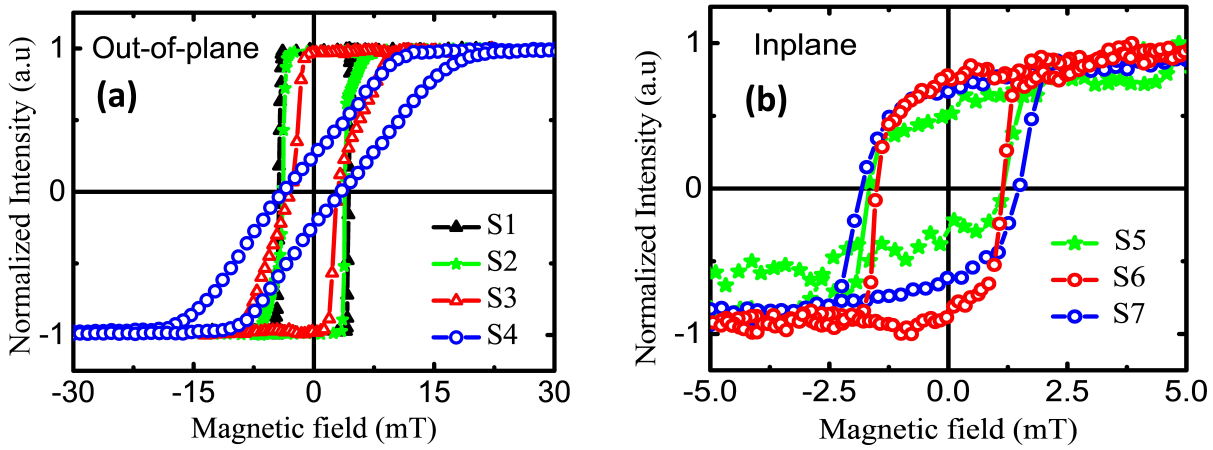


FIG. S1. MOKE hysteresis loop for the samples S1 to S4 (a) and S5-S7 (b) measured at room temperature in polar and longitudinal modes, respectively.

The area between M_s and the in-plane M – H curves represents the effective anisotropy (K_{eff}) of a system [1]. So K_{eff} can be written as, $K_{eff} = -\frac{1}{2}H_sM_s$ (negative sign indicates the IP anisotropy), where H_s and M_s are saturation field, and spontaneous magnetization, respectively. For out-of-plane magnetized samples (S1, S2, S3 and S4), H_s is the intersecting point of saturation field of IP and OOP hysteresis loop (Fig S2 (a)-(d)). For the IP magnetized samples (S5, S6 and S7), H_s is the required field to saturate the film in perpendicular mode (measured by MOKE) which is shown in Fig. S2 (e)-(g).

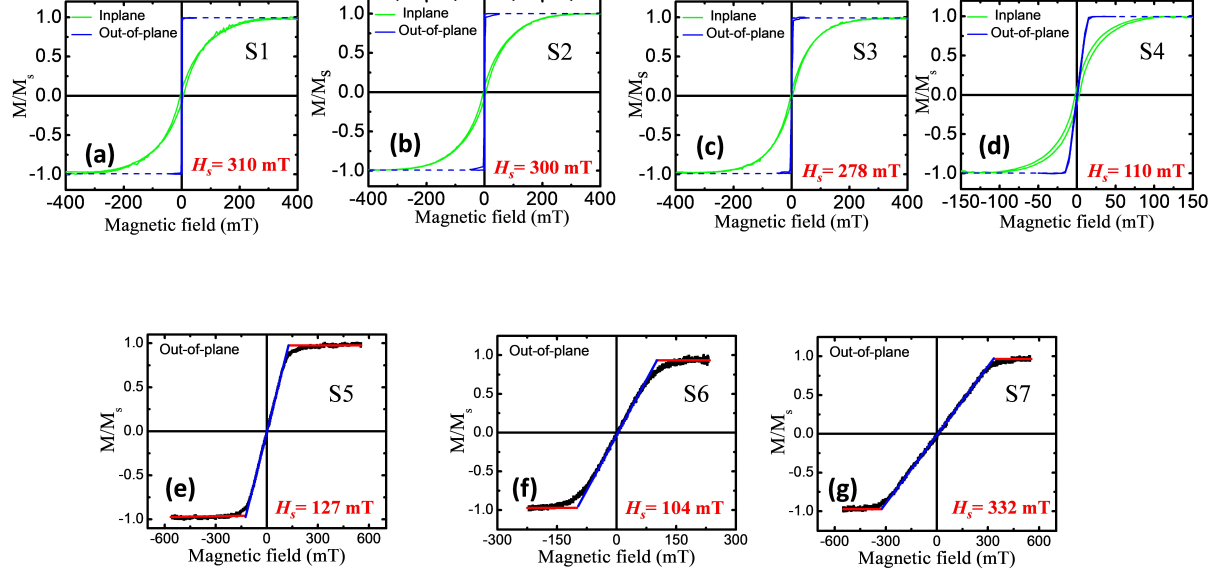


FIG. S2. Hysteresis loops measured by SQUID (for samples S1, S2, S3 and S4) or MOKE (samples S5, S6 and S7) from which the saturation field of all the samples have been evaluated.

In Fig. S3, the saturation magnetic moment per unit area (calculated from the SQUID loops) as a function of CoFeB thickness has been plotted (black dots) and fitted with a linear equation (red line). The fitted line intersects the x -axis at $x = 0.4$ which gives the dead layer thickness (t_d) of the films. Here, dead layer forms mainly due to intermixing at bottom Pt/CoFeB interface and oxidation at top CoFeB/MgO interface. The slope of the linear fits gives the saturation magnetization (1.58×10^6 A/m) of the Pt/CoFeB/MgO heterostructure.

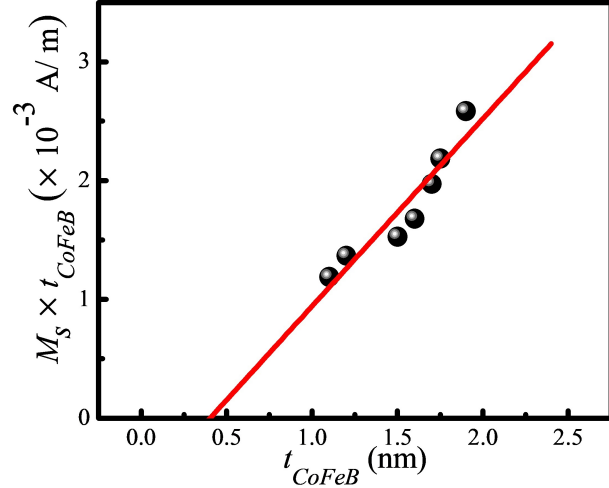


FIG. S3. Plot of saturation moment/area vs CoFeB thickness.

ANALYSIS OF IDMI

Fig. S4 (a) shows the schematic of the measurement geometry using Brillouin light scattering (BLS) in Damon Eshbach (DE) configuration. In this measurement, a horizontally polarised laser beam is incident on a sample surface where the incident photons interact with magnons. The 180° backscattered photons (arises due to inelastic scattering) are sent through a tandem Fabry–Perot (FP) interferometer to achieve a high spectral resolution and to extract the information about spin wave. Stokes (S) and Anti-stokes (AS) peaks arises due to creation and annihilation of the magnons, respectively, in the BLS spectra and the respective spin wave propagates in the opposite direction. The wave vector of the spin wave is represented as $k_{sw} = \frac{4\pi \sin \theta}{\lambda}$, where θ is the incident angle, and λ ($=532$ nm) is the wavelength of incident laser light. Here, a magnetic field has been applied perpendicular to the incident plane of light. Fig. S4 (b) shows the BLS spectra of the sample S4 measured at $k_{sw} = 4.1 \mu\text{m}^{-1}$ and a constant applied field ($\mu_0 H = 371$ mT).

The BLS data have been analyzed using the following spin-wave dispersion relation in DE mode [2–4]

$$f = f_0 \pm f_{DMI} = \frac{\gamma \mu_0}{2\pi} \sqrt{[H + Jk_{sw}^2 + P(k_{sw})M_s][H + Jk_{sw}^2 - P(k_{sw})M_s - H_{K_{eff}}]} \pm \frac{\gamma}{\pi M_S} D_{eff} k_{sw} \quad (1)$$

where, γ is the absolute value of the gyromagnetic factor [$\gamma/2\pi = g \times 13.996$ GHz/T, with g the gyromagnetic factor],

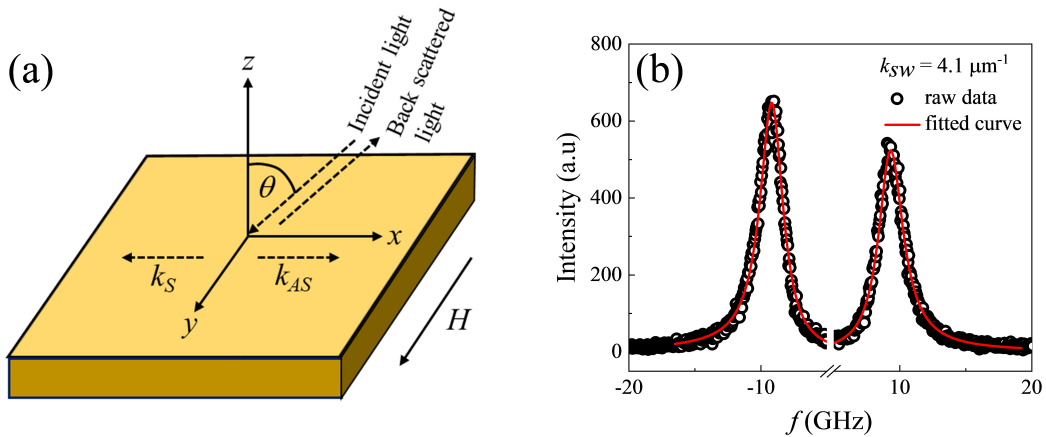


FIG. S4. (a) Measurements geometry of BLS technique. (b) BLS spectra of sample S4 measured at a constant applied field ($\mu_0 H = 371$ mT).

μ_0 is the vacuum permeability, $J = 2A/(\mu_0 M_S)$ is the SW stiffness constant with A the micromagnetic exchange constant, D_{eff} is the effective DMI constant, $H_{K_{eff}}$ is the effective anisotropy, $P(k_{sw}) = 1 - \frac{1 - \exp(-|k_{sw}|t_{CoFeB})}{|k_{sw}|t_{CoFeB}}$. The first part of the above equation, $f_0 = \frac{f_S + f_{AS}}{2}$ (f_S and f_{AS} peak frequencies of S and AS lines of BLS measurements), represents the average spin wave frequency having no iDMI at the HM/FM interface whereas the second part arises due to iDMI.

From equation (1) the frequency difference between S and AS peaks can be written as:

$$\Delta f = f_S - f_{AS} = \frac{2\gamma}{\pi M_S} D_{eff} k_{sw} \quad (2)$$

Δf as a function of k_{sw} has been plotted in Fig. S5 for both the samples. From the slope of linear fit, DMI constant D_{eff} can be deduced. The magnitude of iDMI constants are 0.41 ± 0.025 mJ/m² and 0.39 ± 0.016 mJ/m² for S3 and S4, respectively.

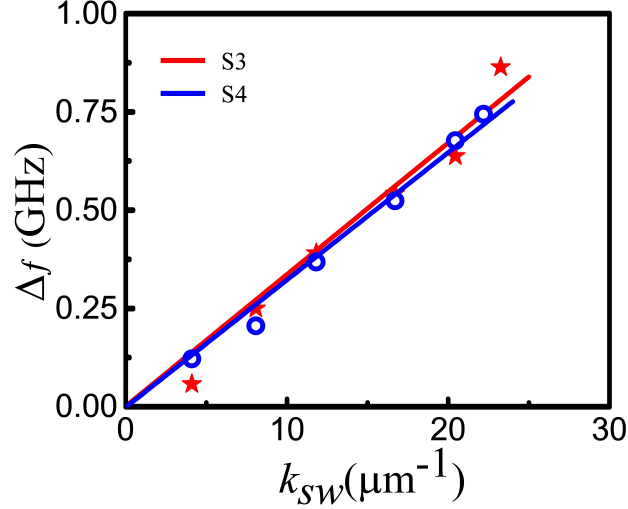


FIG. S5. Plot of frequency difference (Δf) vs spin wave vector (k_{sw}) at $\mu_0 H = 371$ mT

ANALYSIS OF THE PULSE

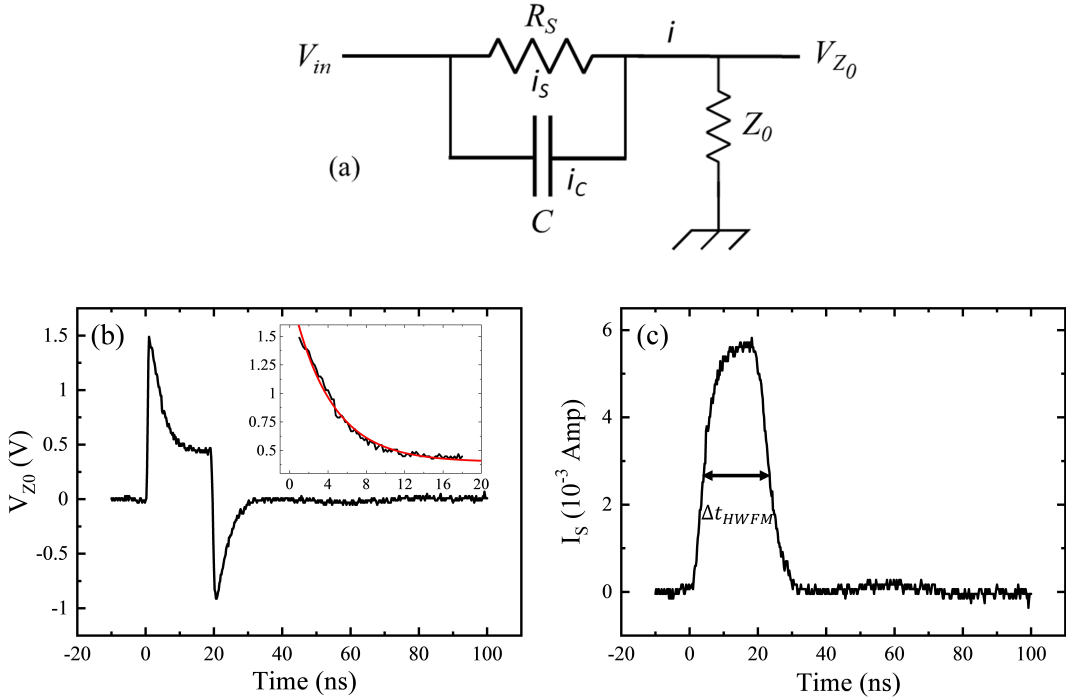


FIG. S6. (a) Circuit diagram of the sample considering capacitive short through the substrate. (b) Shape of the voltage pulse measured on the 50Ω load of an oscilloscope and (c) processed current pulse flowing through the nanotracks, for a 20 ns long 2 V pulse (note that due to the impedance mismatch at the sample, 25% of the pulse is reflected before the sample and does not participate to the pulse).

The Si substrate used in the experiment has the resistivity of $0.01 \Omega\text{cm}$, which is small as compared to the track resistance. While this has no impact in DC, it limits the minimum pulse duration, since the current initially flows

through the substrate. Hence, we can consider the sample as per the circuit diagram presented in Fig. S6(a). The pulse measured on the $50\ \Omega$ load of an oscilloscope does not directly correspond to the current through the tracks, but to the sum of the currents through the substrate and the track. At the beginning of the pulse, the current flows directly through the capacity and the voltage on the load is the one of the pulse. After the transient regime, the current through the capacity is zero and the voltage on the load is $Z_0/(Z_0 + R_S)$. From the measurement in Fig. S6(b), a time constant of 4 ns and a track resistance $R_S = 188\Omega$ are deduced. The current pulse through the sample can be deduced, as shown in Fig. S6 (c). The pulse width is calculated as the full-width at full maxima of the pulse, here 19 ns. The current density through the sample is subsequently calculated by dividing the current with the product of width and thickness of the nanotacks.

* These authors contributed equally to this work

† stanislas.rohart@universite-paris-saclay.fr

‡ sbedanta@niser.ac.in

- [1] M. Yamanouchi, A. Jander, P. Dhagat, S. Ikeda, F. Matsukura, and H. Ohno, Domain structure in cofeb thin films with perpendicular magnetic anisotropy, IEEE magnetics letters **2**, 3000304 (2011).
- [2] M. Belmeguenai, J.-P. Adam, Y. Roussigné, S. Eimer, T. Devolder, J.-V. Kim, S. M. Cherif, A. Stashkevich, and A. Thiaville, Interfacial dzyaloshinskii-moriya interaction in perpendicularly magnetized pt/co/alo x ultrathin films measured by brillouin light spectroscopy, Physical Review B **91**, 180405 (2015).
- [3] S. Tacchi, R. Troncoso, M. Ahlberg, G. Gubbiotti, M. Madami, J. Åkerman, and P. Landeros, Interfacial dzyaloshinskii-moriya interaction in pt/cofeb films: Effect of the heavy-metal thickness, Physical review letters **118**, 147201 (2017).
- [4] K. Di, V. L. Zhang, H. S. Lim, S. C. Ng, M. H. Kuok, X. Qiu, and H. Yang, Asymmetric spin-wave dispersion due to dzyaloshinskii-moriya interaction in an ultrathin pt/cofeb film, Applied Physics Letters **106**, 052403 (2015).